Final Draft
of the original manuscript:

Vaidya, M.V.; Horstmann, M.; Ventzke, V.; Petrovski, B.; Kocak, M.;
Kocik, R.; Tempus, G.:

Structure-property investigations on a laser beam welded dissimilar joint of aluminium AA6056 and titanium Ti6Al4V for aeronautical applications, Part II: Resistance to fatigue crack propagation and fracture

In: Materialwissenschaft und Werkstofftechnik (2009) Wiley

DOI: 10.1002/mawe.200900367

Structure-property investigations on a laser beam welded dissimilar joint of aluminium AA6056 and titanium Ti6Al4V for aeronautical applications

Part II: Resistance to fatigue crack propagation and fracture

Untersuchungen zu Struktureigenschaften von laserstrahlgeschweißten Mischverbindungen aus Aluminium AA6056 und Titan Ti6Al4V für Anwendungen in der Luftfahrt

Teil II: Widerstand gegen Ermüdungsrissausbreitung und Bruch

W. V. Vaidya*[1], M. Horstmann[1], V. Ventzke[1], B. Petrovski[1], M. Koçak[1], R. Kocik[2] and G. Tempus[2]

[1]GKSS Research Centre Geesthacht,
Institute of Materials Research,
Materials Mechanics,
Max-Planck-Strasse 1
D-21502 Geesthacht,
Germany

[2]AIRBUS Deutschland GmbH,
Metal Technology,
Airbus-Allee 1,
D-28199 Bremen,
Germany

*Corresponding author
e-mail: waman.vaidya@gkss.de
Tel.: 0049 4152 872600
Fax.: 0049 4152 872534

Abstract

Investigations were continued on the dissimilar laser beam welds of AA6056 and Ti6Al4V, fabricated by inserting Ti-sheet into the profiled Al-sheet and melting AA6056 alone. By using microstructure, hardness and strength as the criteria, sites exhibiting non-uniform microstructure and localized plastic deformation due to strength mismatch were investigated in two orientations:

- crack parallel to the weld and
- crack perpendicular to the weld

for fatigue crack propagation and fracture toughness at room temperature. Effect of temper of AA6056 on these properties was studied for two conditions; welding in T4 followed by post weld heat treatment T6, and welding in T6 and naturally aged for a defined period. The orientation “crack parallel to the weld” was investigated in 3 locations on the side of AA6056: the interface and the two changeovers on the Al-side. Firstly, between the fusion zone and the heat affected zone (3 mm from the interface) and secondly, between (primary) heat affected zone and towards the base material (7 mm from the interface). Although brittle intermetallic $TiAl_3$ had been formed at the interface, uncontrolled separation or debonding at the interface was not observed. Insofar the bond quality of the weld was good. However, the ranking of interface was the lowest since fatigue crack propagation was relatively faster than that in the fusion zone and heat affected zone, and fracture toughness was low. Therefore, unstable fatigue crack propagation is observed when the crack propagates perpendicular to the weld from AA6056 towards Ti6Al4V. The results have shown that the dissimilar joints exhibit improved performance when laser beam welded in the T6 condition.

Keywords: Aluminium alloy AA6056, Dissimilar weld, Fatigue crack propagation, Fracture, Fractography, Laser beam welds, Titanium alloy Ti6Al4V

Zusammenfassung

Die Untersuchungen an der laserstrahlgeschweißten Mischverbindung aus AA6056 und Ti6Al4V wurden fortgesetzt. Für die Ermüdungsrissausbreitungs- und Bruchzähigkeitsversuche bei Raumtemperatur wurde die Al-seitige lokale Heterogenität des Gefüges, der Härte und Festigkeit als Kriterium für die Festlegung der Risspositionen in den Verbindungen herangezogen:

- Riss parallel zur Schweißnaht und
- Riss senkrecht zur Schweißnaht.

Dabei wurde auch der Einfluss des Laserstrahlschweißens in den Warmauslagerungszuständen T4 und T6 der Al-Legierung AA6056 auf die Ermüdungsrissausbreitung und Bruchzähigkeit beurteilt. Die im Zustand T4 laserstrahlgeschweißte Verbindung wurde mit einer nachfolgenden Warmauslagerung in den Zustand T6 gebracht. Die im Zustand T6 laserstrahlgeschweißte Verbindung wurde nach einer definierten Kaltauslagerungsdauer getestet. Die Orientierung “Riss parallel zur Schweißnaht” wurde in 3 Bereichen auf der Al-Seite untersucht: an der Grenzfläche zwischen AA6056 und Ti6Al4V, zwischen Fügezone und Wärmeeinflusszone (3 mm Abstand von der Grenzfläche) und zwischen Wärmeeinflusszone und Grundwerkstoff (7 mm Abstand von der Grenzfläche). Obwohl sich an der Grenzfläche sprödes $TiAl_3$ gebildet hat, wurde keine Trennung oder Ablösung an der Grenzfläche beobachtet. Insofern war die Bindequalität der laserstrahlgeschweißten Mischverbindung als gut zu bewerten. Allerdings war im Bereich der Grenzfläche die Ermüdungsrissausbreitung schneller als in der Fügezone und der Wärmeeinflusszone und die Bruchzähigkeit vergleichsweise gering. Instabiler Ermüdungsrissfortschritt wurde beobachtet, wenn sich der Riss senkrecht zur Schweißnaht von AA6056 in Richtung Ti6Al4V ausbreitet. Die Ergebnisse haben gezeigt, dass die Mischverbindung einen verbesserten Widerstand aufweist, wenn im T6-Zustand laserstrahlgeschweißt wird.

Schlüsselworte: Aluminiumlegierung AA6056, Mischverbindung, Ermüdungsrissausbreitung, Bruch, Fraktographie, Laserstrahlschweißung, Titanlegierung Ti6Al4V

1 Introduction

Cracks raise the stress concentration locally and reduce the load bearing capacity. Therefore, the allowable stress range to avoid failure under fatigue decreases substantially with the increase in the crack length [1]. This presentation has become known in the fatigue and fracture community as the Kitagawa Diagram and is used to define the safe fatigue region. Dissimilar welds with their complexity [2] originating from local gradients in composition, microstructure and strength are likely to exhibit a location dependent diversity in fatigue and fracture properties. Since cracks can be detrimental for properties, sufficient material resistance is required for cyclic and static loading against premature failure. Fortunately, some defects may be tolerated under loading and the weld interface may not necessarily be a critical site.

Tuppen et al. [3] observed for diffusion-bonded Ti6Al4V-Ti4Al4Mo2Sn (Ti550) joints that non-fusioned small defects at the interface did not affect the fatigue behaviour notably. However, when interfacial defects were large and initiated cracks, fatigue strength was lowered and the life became shorter. Otherwise, the fatigue behaviour of the joint was comparable to that of Ti6Al4V and the fracture during fatigue and tensile test occurred in Ti6Al4V (which was the weaker partner), well away from the bonded interface. Uematsu et al. [4] found on a friction stir welded dissimilar joint of wrought (AA6061-T6) and cast (AC4CH-T6) Al-alloys that casting defects facilitated crack initiation and reduced the fatigue life. When such defects were eliminated by friction stir processing, the fatigue behaviour of the joint was improved to the level of AA6061-T6. A further post-weld heat treatment to T6 rectified the hardness trough (undermatch) within the weld and raised the hardness level nearly to that of the base materials (evenmatch), however, did not bring further improvement in fatigue. These very recent results show that the fatigue behaviour is dependent more on the elimination of defects rather than on the improvement in strength. Wahab and Alam [5] have analysed the effect of fusion weld imperfections on the fatigue life using finite element analysis method and have shown a systematic decrease in the fatigue life in the order of porosity, undercut and solidification cracks. Thus, since welds may contain defects, the crack initiation phase may be short or even absent depending on the load levels. Therefore, to be on the safer side, it is advisable to assume that the whole life shall be limited by fatigue crack propagation and fracture.

Fatigue crack propagation is not a unique but a parameter dependent property and, hence, can be case dependent. For a crack within the weld, the resistance to fatigue crack propagation for strength overmatching in shield metal arc welded butt-joints of a low alloy high strength steel (HSLA80) is found to be superior to that for undermatching [6]. On the other hand, undermatched friction stir welded butt-joints of AA6056-T6 are found to exhibit a nearly comparable fatigue crack propagation behaviour to that of the base material or even better in the nugget region [7]. Moreover, although undermatched, butt-joints of AA6056-T6 are found to exhibit a better resistance to fatigue crack propagation when welded by friction stir than by laser beam [8]. Thus, along with the strength of the weld, the welding process (on which the occurrence of defects depends) and the resulting microstructure can also be decisive in determining the fatigue crack propagation behaviour.

Weld interface is the region where a sharp property changeover occurs [2]. In a friction-welded joint of martensitic-austenitic stainless steel fatigue crack propagation in locations away from the interface was found to be slower than that in the base material [9]. The interface in this case was overmatched. However, in contrast to the behaviour to be expected from that observed in HSLA80 steel [6], faster fatigue crack propagation due to the interface separation was observed. Fatigue crack propagation along the interface between a dissimilar joint of mild steel-austenitic stainless steel is also found to be impaired [10]. Voids and impurities at the interface and secondary cracking facilitated the interfacial debonding in this case and degraded the resistance to fatigue crack propagation. Therefore, the bond quality in terms of weld defects at the interface may overshadow the strength-matching [6-8] effect on fatigue crack propagation.

In the examples cited above the direction of fatigue crack propagation was within [6-8] or parallel [7,9] to the weld or along the interface [9-10]. For dissimilar welds the initial direction of fatigue crack propagation is also found to be influential, when fatigue crack propagation occurs perpendicular to the weld. Suresh et al. [11] have shown on explosively welded ferritic and austenitic steel that when the crack propagates from ferrite (soft/weak) to austenite (hard/strong) the crack slows down (and is arrested) as it approaches the weld interface and is obstructed from crossing the interface. However, when the fatigue crack propagation direction is reversed, such behaviour is no more observed. They explained this phenomenon in terms of cyclic slip which is obstructed when the crack propagates from the softer towards the harder site. In turn, the constraint is decreased and the crack tip is protected due to the decrease in

the driving force. Further experiments, performed also on explosively welded bimetallic pairs, pure iron (ARMCO)-low alloy high strength ferritic steel (SAE4340) [12] and mild steel-austenitic stainless steel (type AISI321) [13-14], have confirmed this phenomenon.

As for fatigue crack propagation, the dissimilar weld interface can also be decisive for the fracture behaviour. In tensile test the interface in an explosively welded mild steel-austenitic stainless steel is found not to be detrimental since the fracture occurred away from the interface in the mild steel [10]. However, when tested for fracture toughness, this interface exhibited lower resistance than both base materials, which is attributed partly to defects at and within the interface. In contrast, a diffusion-bonded dissimilar joint produced by sandwiched pure aluminium foil between pure titanium blocks is found to be non-damaging to the fracture toughness although a thin brittle intermetallic $TiAl_3$ phase (≤ 2 μm) was formed at the joint interface [15]. Interestingly, all specimens, tested in four point bending without fatigue pre-cracking, failed by void formation in the Al-interlayer (457 μm $\leq t_{Al} \leq$ 2000 μm) by ductile fracture. Only when the intermetallic width was deliberately increased to about 8 μm, interface debonding occurred and the specimens failed in the brittle mode.

It would be evident from above that a result may not be unique but modified for a given case, particularly when defects are present, and needs to be verified. In this context cracks provide a critical insight into the material behaviour, which in turn can help for the verification of the weld quality.

Previously, (in Part I [16] of this Paper), local gradients in basic properties of the dissimilar laser beam welds of AA6056 and Ti6Al4V, fabricated by inserting Ti-sheet into the profiled Al-sheet and melting AA6056 alone, were reported. By using microstructure, hardness and strength as the criteria, sites exhibiting non-uniform microstructure and localized plastic deformation were searched for. Thereby three possible critical sites that may initiate failure were identified: the interface and the two changeovers on the Al-side; firstly, between the fusion zone and the heat affected zone (3 mm from the interface) and secondly, between (primary) heat affected zone and towards the base material (7 mm from the interface). With this background fatigue crack propagation and fracture at these sites are investigated here (Part II). Additionally, crack orientation perpendicular [11-14] to the weld is also considered. Effect of temper of AA6056 on properties was studied for two conditions; welding in T4

followed by post weld heat treatment T6, and welding in T6 followed by defined natural ageing.

As in the Part I [16] the terminology “welding” [17] has been retained, since at least one partner was melted (and thus it is not considered as brazing). The partners are also referred to synonymously by the respective side, e.g., AA6056 as the Al-side. Moreover, specimens from the laboratory coupons (and not the component in Fig. 1c in Part I [16]) have been tested. To avoid reshuffling, some salient features from the Part I are recalled at appropriate places.

2 Experimental procedure

Information on the welds and their basic characteristics are reported in Part I [16]. In brief, sheets of the precipitation hardenable AlMgSiCu type alloy AA6056 (uniform thickness 2 mm) and Ti6Al4V (thickness 1.8 mm; mill annealed) were welded to coupons using a split beam 4 kW Nd:YAG laser in the heat conduction mode without using filler wire. The coupon had the dimensions 330 x 94 mm^2. To study the effect of starting microstructure on properties two tempers were selected for AA6056:

- welding in T4 followed by artificial ageing T6 (190 °C-4h/air); denoted also as “T4/T6” or “T4 followed by post weld heat treatment T6”, and
- welding in T6 and defined naturally aged (at least for 7 weeks) without any further artificial ageing; denoted also as “T6” without a special reference to the natural ageing.

Compact tension [18], C(T), specimens with the initial notch length, a_n = 10 mm, the specimen width, W = 50 mm and as-welded full thickness (= B) were tested. Fatigue crack propagation specimens had a straight notch. Specimens for fracture toughness testing had similar dimensions but the notch was modified in the load line for a gauge insertion and the distance between the loading holes was longer [18]. At least two specimens for a given variant were tested to improve the data reliability. All welded specimens were tested with the excess weld material (see Fig. 2 to follow), except for that removed during surface polishing as required for optical crack length measurement. For comparison, base material specimens were tested for baseline data and had the same dimensions as those for the weld.

Specimens were extracted by electric discharge machining in two locations: parallel to the weld and perpendicular to the weld, as shown in Fig. 1 for fatigue crack propagation specimens. Specimens for fracture toughness were extracted in a similar way. For specimens parallel to the weld, three individual locations were selected (see Part I [16]) and are shown in Fig. 2. In brief, the location “3 mm from the interface” was in the first changeover between fusion zone (cast microstructure) and heat affected zone (wrought microstructure) and “7 mm from the interface” between (primary) heat affected zone and the base material AA6056. This latter location had the lowest hardness, irrespective of in which temper the joint was welded. For specimens perpendicular to the weld, the crack was made to propagate from AA6056 over the primary heat affected zone, fusion zone and the interface before entering into Ti6Al4V in one case, and vice versa in the other. Therefore, the distance between the notch and the interface was more (10 mm) than that for the crack propagating from Ti6Al4V into AA6056 (5 mm). In the latter case the notch was away from the cusped excess aluminium on titanium.

After cutting and machining, the initial bending was reduced but was still present. So as to avoid effect of bending and near zero or below zero loading, a high load ratio value, R (= P_{min}/P_{max}), was used for fatigue crack propagation testing and P_{min} value controlled closely. The average R value was 0.4 ± 0.05. Specimens were tested using servo-hydraulic machines at a frequency f = 10 Hz and under ambient laboratory conditions at room temperature. The standard ASTM E647 [18] was followed for specimen dimensions and testing. It must be mentioned here that this testing standard assumes homogeneous material properties (a condition, which may not necessarily be applicable to the welded joints). The starting ΔK value for all specimens at the beginning of the test was the same and was 10 MPa$\sqrt{m}$. The data up to a crack length a = 24 mm was considered for presentation, although data were acquired over a longer crack length. Crack length was measured indirectly and continuously by using an on-top extensometer for maximum crack opening displacement (COD_{max}) and calibrated against the optical crack length. A typical example is shown in Fig. 3. The polynomial was then used for crack length calculation. Such polynomial was obtained for each specimen. The advantage here is that the test could be automated and more data points were obtained.

For fracture toughness testing of “crack perpendicular to the weld” the initial notch length, a_n, was extended by fatigue pre-cracking ($\Delta a \geq 2.5$ mm) to introduce a

sharp crack and to reach the value 0.5 W (= 25 mm). Specimens were tested using servo-hydraulic and electro-mechanical machines in the laboratory air and at room temperature using the GKSS procedure [19]. This procedure is similar to that by ASTM E561 [18] but is modified additionally by a local crack tip opening displacement (CTOD δ_5) technique [20] (shown in Fig. 12 to follow). The advantage is that the information is obtained *directly* on the crack tip and does not have to be inferred from the load line gauge, which is particularly important for the dissimilar joint as in the present case. Hence, local CTOD values are used to describe the fracture toughness.

Extensive fractographic investigation was undertaken to understand the failure process. Thereby for the interface specimens the fracture half of Ti-side was examined, since it was easier to identify adhering Al-particles and thus assess the bond characteristics.

3 Results and discussion

The resistance to fatigue crack propagation is conventionally represented by the rate of crack propagation, da/dN, against the stress intensity range, ΔK. Thereby the material homogeneity and global elastic deformation are tacitly assumed. When a crack propagates perpendicular to the interface of a dissimilar weld, before and after crossing the interface the crack propagates in only one partner of the weld. Hence, questions in the context of K-concept applicability do not turn up and the results [11-14] are presented in the conventional way. Furthermore, these literature data [11-14] are obtained on steels, for which the Young's moduli are nearly the same (200 ± 10 GPa). For the present case of the bimetallic joint with very different Young's moduli we have not yet assessed the K-field by finite element analysis. Therefore, for the time being we assume the K-concept applicability as the crack propagates in homogeneous Ti6Al4V (Fig. 11 to follow) but when fatigue crack propagation occurs over various non-homogeneous microstructural zones in AA6056, fatigue crack propagation data are presented in terms of crack length (in Fig. 10 to follow).

When a crack propagates parallel to a dissimilar weld, the partners on either side are different and in cases other than steels, also have different Young's moduli, as in the present case. To exclude discussions on the K-concept applicability in this case, fatigue crack propagation results are presented in terms of crack length (on log-log scale). The starting condition being the same for all tests and ΔK being a function of

crack length, this approach should suffice for the internal comparison of results. In contrast to fatigue crack propagation tests, for fracture toughness tests questions about the K-concept applicability do not turn up when the elastic-plastic fracture toughness value is determined by using CTOD δ_5 technique [20], and the latter is used as the evaluating parameter.

Fatigue crack propagation data on the base materials are shown in Fig. 4 in two orientations; along the rolling direction (TL) and perpendicular to it (LT). Compared to Ti6Al4V, the difference in fatigue crack propagation in AA6056-T6 is insignificant in both orientations, which is an effect related partly to the crystal structure. Deformation in a hexagonal close packed structure (Ti6Al4V) is due to limited slip systems more orientation-dependent than that in a face cubic centre structure (AA6056). Moreover, AA6056-T6 is found to be slightly more sensitive to fatigue crack propagation than Ti6Al4V. These data are shown in the figures to follow as a band and are used as the reference for comparison.

3.1 Fatigue crack propagation behaviour

3.1.1 Fatigue crack propagation parallel to the weld

In general, fatigue crack propagation in the Paris regime (as investigated here) is insensitive to a number of parameters. Nonetheless, some microstructural influence depending on the ageing has been found in 6XXX Al-alloys [21-23]. Resistance to fatigue crack propagation in the underaged condition (T4; GP zones) is found to be better than that in the peakaged condition (T6; β" precipitates), both for the base material and the laser beam welded butt-joints of AA6056 [21-22]. Moreover, overageing (β" → β'/Q' precipitates) in the heat affected zone of a comparable alloy has been found to provide a fatigue crack propagation behaviour as good as to that in the base material [23]. Thus, a type of precipitates that improves strength and hardness (e.g., β") may not necessarily improve the fatigue crack propagation behaviour. For that purpose a condition amenable for deformation such as underageing or overageing would be more favourable.

It follows that when a crack propagates through a gradient having different types of precipitates, its fatigue crack propagation response shall change depending on the local microstructural gradient. To recall the salient features of the locations

investigated [16], the interface was found to be strong, irrespective whether under constraint (macro-tensile specimens) or nearly free from it (microflat-tensile specimens). The tensile fracture occurred well away from the interface and in AA6056. The microstructure varied from wrought (heat affected zone; “7 mm” site) to cast (fusion zone; “3 mm” site). But irrespective of the temper in which the joint was welded, the macro-tensile fracture occurred within the hardness dip in the heat affected zone at “7 mm” site. This site was overaged (stable β/Q precipitates) with hardness increasing on either side (due to β’/Q’). The extent of increase in the hardness towards the fusion zone differed in T4/T6 (β’/Q’ + β”) and T6 (β’/Q’) but the hardness trend in the secondary heat affected zone towards the base material was similar (β’/Q’ with increase in β”). Thus, T4/T6 contained more β” at the locations investigated and hence, should be more sensitive to fatigue crack propagation.

The fatigue crack propagation data at various notch locations are shown in Figs. 5-6. The locations on the Al-side had a uniform thickness (2 mm). In contrast, the location interface was curved due to the excess in AA6056 and being thicker locally, should have experienced less driving force (see the inset in Fig. 6). Also the crack had to propagate over excess thickness; interface in the mid-thickness (brittle) and excess AA6056 (ductile) on either side. Nonetheless, fatigue crack propagation at the interface is found to be faster than that at other locations. The effect of crack propagating in a hardness dip with the gradient on either side is seen as scatter in the data, which is more at “7 mm” than that at “3 mm” or the interface (Figs. 5-6). Thereby welding in the T6 temper is found to offer a higher resistance to fatigue crack propagation at “3 mm” (GP zones) and the interface (β’/Q’) than that in the T4 temper followed by post weld heat treatment T6 (β”). Thus, as regards the resistance to fatigue crack propagation, underageing or overageing turns out to be more beneficial than peakageing [21-23]. It also needs to be mentioned that at the interface stable fatigue crack propagation was observed (and not uncontrolled separation or debonding) and when welded in T6, the fatigue crack propagation response was as good as that of AA6056. The crack appearance on the surface is shown in Fig. 7 for various locations. At “7 mm” and “3 mm” the crack propagated initially straight but thereafter deviated and deflected substantially. This is attributed to local variations in the hardness gradient [16] and hence, to the difference in the deformation behaviour on either side of the crack. The crack at the interface remained, however, straight.

A remarkable feature in fatigue crack propagation was the steeper slope after initial stabilization, both in T4/T6 and in T6 (Fig. 5). Assuming for the time being the applicability of the ΔK-concept, the fractographic features are shown after the stabilization (ΔK = 12 MPa$\sqrt{m}$) and in the mid-curve (ΔK = 15 MPa$\sqrt{m}$) in Fig. 8. Whereas the base material AA6056-T6 is found to exhibit mainly striations over the entire fatigue crack propagation region (Figs. 8a-b), the weld at "3 mm" location (fusion zone) is found to exhibit a combined fracture mode; striations (fatigue mode) and dimples (ductile tear mode), Figs. 8c-d. With the increase in crack length (which is equivalent to the increase in ΔK) cracks formed in striations (Fig. 8b) and the proportion of dimples increased (Fig. 8d). Thus, there was a change in the fracture mode in the weld but not in the base material AA6056. Tearing is an effect related to local weak sites in "3 mm" location. Therefore, when the strength is exceeded locally, mainly dimples are observed, the crack propagates faster than in the striation mode and contributes to the increase in the slope of the fatigue crack propagation curve.

Interface is found to be a critical site in dissimilar joints and to exhibit fast fatigue crack propagation due to debonding or interfacial separation [9-10]. In the present case a thin (< 2 μm) brittle intermetallic phase, $TiAl_3$, was formed at the interface [16] and has certainly contributed to an increase in fatigue crack propagation (Fig. 6). Formation of the intermetallic is a high temperature process and (compared to a range compound, e.g., Ti_3Al) particularly $TiAl_3$, being a line compound, can no more be altered during cooling. The only change that occurs during the post weld heat treatment is the formation of secondary metastable precipitates (β"). As mentioned above, β" increases the sensitivity to fatigue crack propagation. Fractographic features over the mid-thickness and at a comparable fatigue crack propagation rate (= 10^{-6} m/cycle) are shown in Figs. 9a-b for T4/T6 and T6. The matrix is Ti6Al4V and the white fragments were found by energy dispersive X-ray (EDX) analysis to contain Al, Mg, and Si (i.e., AA6056). T6 contained more such fragments than T4/T6. Moreover, when welded in T6, β" overages to further variants (β'/Q', β/Q) which makes the matrix more deformable. Near to the interface all the metastable precipitates are expected to dissolve (see Fig. 9 in Part I [16]) which in turn should improve the deformation capacity further and thus contribute to reduction in fatigue crack propagation for the T6 weld (Fig. 6). Deformation traces *were* visible in Ti6Al4V and the joint exhibited *stable* fatigue crack propagation. Thus, this was *not* a brittle interfacial separation, as is evident in Fig. 9a-b. In this sense the weld quality was good.

Occasionally, individual macro-pores were found. It was previously observed [24] in a laser beam welded AA6056-T6 butt-joint that isolated macro-pores are not necessarily detrimental for fatigue crack propagation; on the contrary, they induce crack retardation. This was also confirmed in the present case and is shown in Fig. 9c. Whereas the surrounding is relatively devoid of deformation, before cutting the macro-pores the crack front has been obstructed and has left traces of deformation, since macro-pores act as barrier to the propagating crack front. This was no more observed once the pore was overcome.

Thus, although a brittle intermetallic phase was formed at the interface, fatigue crack propagation occurred (without unstable failure) and the joint exhibited reasonable resistance to fatigue crack propagation in the order “3 mm”, “7 mm” and the interface. A higher resistance was observed in T6 welded specimens than that in T4 followed by post weld heat treatment T6. Thus, welding in T6 is a better variant. In that case the interface specimens are found to exhibit a fatigue crack propagation behaviour which varies between that of both base materials and even over a long crack length range. Since fatigue crack propagation is determined mainly by the interface, it can be expected that by reducing the interfacial area, the resistance to fatigue crack propagation can be improved further. In this context, our on-going work has yielded encouraging results on modified interface.

3.1.2 Fatigue crack propagation perpendicular to the weld

Compared to the crack along the weld, according to the literature [11-14] the variant “crack perpendicular to the weld” should not be that critical since the crack can slow down or even get arrested when it propagates from the softer side. We follow the literature nomenclature [11-14] for bimetallic joints “soft/weak” and “hard/strong” here. The crack was made to propagate presently

- from the Al-side (soft/weak) towards the Ti-side (hard/strong) and
- from the Ti-side (hard/strong) towards the Al-side (soft/weak)

as indicated in Fig. 1.

The crack could be made to propagate from the Al-side, however, on reaching the interface became unstable and propagated along the interface. Therefore, only limited data could be obtained and are shown in Fig. 10. The data obtained on the welded specimens are certainly better than those for AA6056-T6 and, except for the

interfacial fracture, are thus encouraging. A specific difference between T4/T6 and T6 could not be observed initially (“7 mm” zone) but at a later stage (“3 mm” zone). Although the crack should have been retarded due to obstruction of cyclic slip [11], contrary to expectations a permanent arrest did not occur. Instead, the unstable failure occurred along the interface. Insofar, this variant can be critical.

Contrary to the case of fatigue crack propagation from the soft side, crack should propagate unhindered through the interface when started from the hard side [11-14]. This literature trend could be confirmed here only under specific conditions when the crack was made to propagate from the Ti-side. The data are shown in Fig. 11. Although the Young’s moduli differed in our joint, we assume for the time being the applicability of the ΔK concept as in the literature [11-14], at least so long the crack propagates in the Ti-side.

In all specimens (the base material Ti6Al4V being included) the crack could be made to propagate at a starting ΔK value of 10 MPa$\sqrt{m}$. In the case “Ti6Al4V towards AA6056”, however, the crack could not be made to propagate from the notch on the Ti-side even after ten million cycles, neither at 10 MPa$\sqrt{m}$ nor even when ΔK was increased to 15 MPa$\sqrt{m}$. Such non-propagation (which is depicted better in da/dN-ΔK than in da/dN-a or a-N diagram) is indicated by the downward arrows in Fig. 11, and is not observed in the literature [11-14] for the harder side. With the further increase to 20 MPa$\sqrt{m}$ the crack could be initiated but the rate was too fast and the slope too steep. Finally, after crossing the interface and some additional fatigue crack propagation over about 10 mm from the notch, unstable fracture occurred under the fatigue loading. That the fatigue crack propagation curve was shifted clearly to high ΔK values may have different reasons. The distance between notch and the interface was only 5 mm (see Fig. 1) and therefore, the near-notch area had already higher thickness. This should have contributed to the reduction of ΔK. Whether also crack tip blunting occurred and contributed to stress relaxation needs to be investigated. The residual stresses immediate to the interface on the Ti-side were compressive [16]. This may also be the reason for difficulty in crack initiation and propagation at the notch.

It is evident that the case of the crack from “Ti6Al4V towards AA6056” as investigated or even “AA6056 towards Ti6Al4V” (at least in part, except for the instability at the interface) is certainly not critical.

3.2 Fracture toughness

The inset in Fig. 11 is an example that depicts the importance of fracture toughness. This specimen was actually being tested under fatigue loading and after a critical crack length was reached, fractured without any further increase in the load as reported above. Therefore, a material should possess sufficient fracture toughness and be able to resist unstable fracture. Fracture toughness tests [19-20] were conducted using full thickness and original weld geometry. Load vs. CTOD δ_5 curves were obtained on C(T) specimens and CTOD δ_5 at the maximum load F_{max} was taken as a measure of the resistance to fracture. The higher the CTOD δ_5 value observed, the higher is the fracture toughness and the resistance to fracture. Since variation in local microstructure and crack deflection may affect CTOD δ_5 value and contribute to scatter, multiple specimens were tested to obtain a reliable trend.

As for fatigue crack propagation the same locations shown in Fig. 2 for “crack parallel to the weld” were tested and the results are shown in Fig. 12. As to be expected, there is scatter in the data. Nonetheless, the results show the trend that the locations “interface” and “3 mm” (changeover from the fusion zone to the heat affected zone) exhibit lower fracture resistance in T4/T6 than that in the location “7 mm” (changeover from the primary heat affected zone to the base material). Moreover, there is also a certain dependency on the temper in which the joint is welded. Welding in T6 condition is found to improve the fracture toughness of weld region in general. That the CTOD δ_5 values at “7 mm” are nearly comparable in both tempers is due to the hardness dip and the microstructure, which were comparable [16] in both cases. As for fatigue crack propagation, β” in T4/T6 is found to be unfavourable for fracture toughness. On the other hand, overageing and dissolution of precipitates in T6 welds and in the hardness dip at “7 mm” are favourable due to improved amenability to deformation. The latter location was substantially strength undermatched and therefore exhibits higher fracture toughness than both base materials.

Fractographic features are shown in Fig. 13. The interface was found to exhibit a flat fracture in T4/T6, which indicates practically very poor deformation, although when welded in T6, a slight improvement occurred. Nonetheless, (uncontrolled) debonding was not observed despite the formation of the brittle intermetallic $TiAl_3$. As in fatigue crack propagation, the interface turned out to be a more sensitive site. Away from the interface and towards AA6056, the tendency for deformation increased, which

is seen as the occurrence of dimples (ductile fracture mode) in Figs. 13b,d and explains the difference in the fracture toughness behaviour in Fig. 12.

Thus, as for fatigue crack propagation, it follows that the properties of the interface should be improved further, for example, through microstructural modification or design or both. As already mentioned, our efforts in uplifting the resistance to fatigue crack propagation and fracture by design have been fruitful.

The configuration “crack perpendicular to the weld” was also tested for fracture toughness by placing the notch location in AA6056 and in Ti6Al4V respectively. The data are shown in Fig. 14. When the crack extended from Ti6Al4V towards AA6056 the resistance to fracture was lower than that in the opposite case. Among the base materials AA6056-T6 had lower fracture toughness than Ti6Al4V. Thus, when the crack extends into the other partner, fracture toughness of that partner becomes deciding. In addition, the crack extending from Ti6Al4V towards AA6056 traversed various zones in AA6056 such as the interface, the fusion zone and the heat affected zone. Therefore, the fracture toughness was lower. Thus, this latter configuration deserves more attention than when the crack extends from AA6056 towards Ti6Al4V.

That various crack locations could be investigated successfully by conventional tests indicates itself that the present dissimilar joint had good properties.

4 Conclusions

So as to obtain a critical insight into the performance of the dissimilar laser beam weld AA6056 and Ti6Al4V, various locations with

- crack parallel to the weld and
- crack perpendicular to the weld

were investigated for fatigue crack propagation and fracture toughness at room temperature. The results have led to the following conclusions:

1. For the orientation “crack parallel to the weld”, stable fatigue crack propagation was observed at all locations investigated. The location “interface” was found to exhibit the lowest resistance to fatigue crack propagation. Fracture resistance was also low at the interface and is attributed to the formation of brittle intermetallic $TiAl_3$ at the interface.

2. Although brittle intermetallic $TiAl_3$ was formed at the interface, uncontrolled debonding was not observed. Moreover, the bond region did show traces of deformation and insofar the bond quality of the weld was good. Individual macro-pores were found occasionally, had, however, no damaging effect on fatigue crack propagation and fracture.
3. At locations other than the interface, a combined fracture mode, fatigue and tearing, was observed which contributed to steeper slope of the fatigue crack propagation curve.
4. The condition “laser beam welding in T4 followed by post weld heat treating to T6” was found to be tendential inferior in fatigue crack propagation and fracture to that “laser beam welded in T6”. This is attributed to formation of β” precipitates which contribute to increase in the strength but decrease the deformation in the former condition. In contrast, when welded in T6 there is overageing and dissolution of precipitates, due to which deformation is improved.
5. For the orientation “crack perpendicular to the weld” fatigue crack propagation did occur from AA6056 towards Ti6Al4V. However, as the crack hit the interface, a 90° crack turning occurred and fast failure occurred along the interface. In contrast, the case of crack propagation from Ti6Al4V towards AA6056 was not that critical since non-propagation was observed.
6. The crack extending from Ti6Al4V towards AA6056 traversed various zones in AA6056 such as the interface, the fusion zone and the heat affected zone. Therefore, the fracture toughness was lower than that in the opposite case.
7. Since the ranking of properties at the interface is the lowest, it follows that the properties of the interface should be improved by appropriate measures, so that the resistance to fatigue crack propagation and fracture can be improved further.

Acknowledgements

This work was funded by AIRBUS and additionally by GKSS Research Centre. We gratefully acknowledge this financial support.

Literature

1. H. Kitagawa and S. Takahashi: Application of fracture mechanics to very small cracks or cracks in early stages, in Proc. Int. Conf. on Mechanical Behaviour of Materials-ICM2, Boston, ASM, **1976**, pp. 627-631.
2. N. Bailey: Review of metallurgical problems in dissimilar metal welding, in *Welding Dissimilar Metals*, (ed. N. Bailey), The Welding Institute, Cambridge, Great Britain, **1986**, pp. 1-6.
3. S. J. Tuppen, M. R. Bache and W. E. Voice: A fatigue assessment of dissimilar titanium alloy diffusion bond, *Int. J. Fatigue*, **2005**, 27, pp. 651-658.
4. Y. Uematsu, Y. Tozaki, K. Tokaji and M. Nakamura, Fatigue behaviour of dissimilar friction stir welds between cast and wrought aluminium alloys, *Strength Mater.*, **2008**, 40, pp. 138-141.
5. M. A. Wahab and M. S. Alam: The significance of weld imperfections and surface peening on fatigue crack propagation life of butt-welded joints, *J. Mater. Process. Tech.*, **2004**, 153-154, pp. 931-937.
6. S. Ravi, V. Balasubramanian and S. Nemat Nasser: Effect of mis-match ratio (MMR) on fatigue crack growth behaviour of HSLA steel welds, *Engng. Fail. Anal.*, **2004**, 11, pp. 413-428.
7. W. V. Vaidya, K. Angamuthu, V. Ventzke, M. Koçak and F. Palm: Fatigue and fracture behaviour of friction stir welded aluminium alloy AA6056-T6, in *ICAF 2003, Fatigue of Aeronautical Structures as an Engineering Challenge*, (ed. M. Guillaume), Proc. 22nd Symposium of International Committee on Aeronautical Fatigue (ICAF), Lucerne, Switzerland, 5-9 May 2003, Engineering Materials Advisory Service (EMAS), Sheffield, UK, **2004**, pp. 279-296.
8. M. Koçak and W. V. Vaidya: Laser beam and friction stir welding of aluminium alloys: process – property – performance (3p) relationship, in *Laserstrahlfügen: Prozesse, Systeme, Anwendungen, Trends*, (Strahltechnik, Band 19, eds. G. Sepold and T. Seefeld), Proc. 25th Anniversary Meeting, Laser-Anwendungsforum, BIAS Bremen, 12-13 Sept. 2002, Bremen, BIAS Verlag, Bremen, Germany, **2002**, pp. 225-235.
9. D. G. Lee, K. C. Jang, J. M. Kuk and I. S. Kim, Fatigue properties of inertia dissimilar friction-welded stainless steels, *J. Mater. Process. Technol.*, **2004**, 155-156, pp. 1402-1407.

10. F. Jiang, Z. L. Deng, J. Sun and J. F. Wei: Crack propagation resistance along strength mismatched bimetallic interface, *J. Mater. Engng. Perform.*, **2004**, 13, pp. 93-98.
11. S. Suresh, Y. Sugimura and E. K. Tschegg: The growth of a fatigue crack approaching a perpendicularly-oriented, bimaterial interface, *Scr. Metall. Mater.*, **1992**, 27, pp. 1189-1194.
12. R. Pippan, K. Flechsig and F. O. Riemelmose: Fatigue crack propagation behavior in the vicinity of an interface between materials with different yield stresses, *Mater. Sci. Engng. A*, **2000**, A283, pp. 225-233.
13. F. Jiang, W. Kang, K. Zhao, J. Sun, C. Yan, L. Ye and Y.-W. Mai: Experimental investigation on fatigue crack growth normal to a bimaterial interface, in *Structural Integrity and Fracture*, (eds. A. V. Dyskin, X. Hu and E. Sahouryeh), Proc. Int. Conf., Perth, Australia, 25-27 Sept. 2002, A. A. Balkema Publishers, Lisse, The Netherlands, **2002**, pp. 137-140.
14. F. Jiang, Z. L. Deng, K. Zhao and J. Sun: Fatigue crack propagation normal to a plasticity mismatched bimaterial interface, *Mater. Sci. Engng. A*, **2003**, A356, pp. 258-266.
15. G. Cam, M. Koçak, D. Dobi, L. Heikinheimo and M. Siren: Fracture behaviour of diffusion bonded bimaterial Ti-Al joints, *Sci. Technol. Weld. Joining*, **1997**, 2, pp. 95-101.
16. W. V. Vaidya, M. Horstmann, V. Ventzke, B. Petrovski, M. Koçak, R. Kocik and G. Tempus: Structure-property investigations on a laser beam welded dissimilar joint of aluminium AA6056 and titanium Ti6Al4V for aeronautical applications; Part I: Local gradients in microstructure, hardness and strength, *Mater. Sci. Engng. Technol. (Mat.-wiss. u. Werkstofftech.)*, **2009**, XX, pp. XX-XX.
17. S. P. Parker (ed.): *McGraw-Hill Dictionary of Scientific and Technical Terms*, 4th edition, New York, USA, McGraw-Hill Book Company, **1989,** 2056.
18. *Annual Book of ASTM Standards*, Section Three: Metals Test Methods and Analytical Procedures; Volume 03.01: Metals-Mechanical Testing; Elevated and Low-Temperature Tests; Metallography, ASTM International, West Conshohocken, PA, USA, **2005**, **(**E561) pp. 557-569 and (E647) pp. 628-670.
19. K.-H. Schwalbe, J. Heerens, U. Zerbst, H. Pisarski and M. Koçak: EFAM GTP 02-The GKSS test procedure for determining the fracture behaviour of materials, GKSS Report **2002**/24.
20. K.-H. Schwalbe: Introduction of δ_5 as an operational definition of the CTOD and its practical use, *ASTM STP 1256*, **1995**, pp. 763-778.

21. W. V. Vaidya, K. Angamuthu and M. Koçak: Effect of load ratio and temper on fatigue crack propagation behaviour of Al-alloy AA6056, in *FATIGUE 2002*, Proc. 8th Int. Fatigue Congress, 3-7 June 2002, Stockholm, Sweden, (ed. A. F. Blom), Engineering Materials Advisory Service (EMAS), West Midlands, UK, **2002**, pp. 1467-1474.
22. W. V. Vaidya, M. Koçak, E. Seib, H. Assler and J. Hackius: Mechanical behavior of laser beam and friction stir welded aluminium alloys for airframes, *Welding in the World*, **2006**, 48**,** Special Issue No. 7, pp. 261-273.
23. W. V. Vaidya, K. Angamuthu, M. Koçak, R. Grube and J. Hackius: Strength and fatigue resistance of laser-MIG hybrid butt welds of an airframe aluminium alloy AA6013, *Welding in the World*, **2006**, 50**,** No. 11/12, pp. 88-97.
24. W. V. Vaidya, M. Koçak, M. Horstmann, V. Ventzke, M. Pakdil and J. Hackius: Effect of porosity on fatigue crack propagation behaviour of a laser beam welded aluminium alloy, Proc. Int. Conf., *Fatigue Design 2005*, November 16-18, 2005, Centre Technique des Industries Mécaniques, Cetim, (French Industrial and Mechanical Technical Centre), Senlis, France, CD-ROM (ISBN: 2-85400-771-9), **2007**.

Figure captions

Figure 1. Location of fatigue crack propagation specimens with “crack parallel to the weld” and “crack perpendicular to the weld”. Specimens for fracture toughness were extracted similarly. (Dimensions in mm).

Abbildung 1. Probenentnahme für Ermüdungsrissausbreitungsversuche mit den Orientierungen “Riss parallel zur Schweißnaht” und “Riss senkrecht zur Schweißnaht”. Die Proben zur Bestimmung der Bruchzähigkeit wurden auf ähnliche Weise entnommen (Maße in mm).

Figure 2. Relative location of sites for “crack parallel to the weld”, at which notable changes in microstructure, hardness, strength and deformation behaviour were observed. Vertical lines denote the sites which were notched for fatigue crack propagation and fracture testing. The continuation of the primary heat affected zone as a secondary zone is indicated by the arrow.

Abbildung 2. Die verschiedenen Bereiche auf der Al-Seite, in denen hinsichtlich Festigkeit, Härte und Gefüge Änderungen beobachtet wurden, sind durch vertikale Linien gekennzeichnet. Diese entsprechen Positionen auf den Proben für Ermüdungsrissausbreitungs- und Bruchmechanikversuche, in welche Kerben und Risse künstlich eingebracht wurden.

Figure 3. A typical example of the relationship between the maximum crack opening displacement and the optical crack length during fatigue crack propagation in a laser beam welded specimen in T6 with “crack parallel to the weld” and in the fusion zone. The fitted polynomial was used as the calibration curve for indirect crack length measurement. The position of the displacement gauge is shown in the inset.

Abbildung 3. Ein typisches Beispiel für die Beziehung zwischen maximaler Rissöffnung und Rissverlängerung während der Ermüdungsrissausbreitung in einer im Zustand T6 laserstrahlgeschweißten Probe mit der Orientierung “Riss parallel zur Schweißnaht”. Für eine indirekte Risslängenmessung wurde die durch ein Polynom angepasste Kurve zur Kalibration herangezogen. Das eingefügte Bild zeigt schematisch die Lage des Dehnungsmessaufnehmers.

Figure 4. Fatigue crack propagation behaviour of the base materials along the rolling direction (TL orientation) and perpendicular to it (LT orientation). The range of fatigue crack propagation of the base materials is shown by hatching and is used for comparison in the diagrams to follow.

Abbildung 4. Ermüdungsrissausbreitung in den Grundwerkstoffen parallel zur Walzrichtung (TL) und quer zur Walzrichtung (LT). Der jeweilige Bereich der Ermüdungsrissausbreitung ist schattiert hervorgehoben und wird in nachfolgenden Diagrammen zur besseren Vergleichbarkeit hinterlegt.

Figure 5. Fatigue crack propagation behaviour for “crack parallel to the weld” at the locations shown in the insets on the side of AA6056, laser beam welded in the T4 condition followed by post weld heat treatment T6, and welded in the T6 condition and defined naturally aged for notch location “7 mm from the interface” (a), and “3 mm from the interface” (b).

Abbildung 5. Ermüdungsrissausbreitung parallel zur Schweißnaht in verschiedenen Risspositionen bei 7 mm (a) und 3 mm (b) auf der AA6056-Seite, im Zustand T4 laserstrahlgeschweißt und anschließend warmausgelagert in den Zustand T6 sowie laserstrahlgeschweißt im Zustand T6 und definiert kaltausgelagert.

Figure 6. Fatigue crack propagation behaviour for “crack parallel to the weld” at the interface, laser beam welded in the T4 condition followed by post weld heat treatment T6, and welded in the T6 condition and defined naturally aged.

Abbildung 6. Ermüdungsrissausbreitung parallel zur Schweißnaht an der Grenzfläche der Verbindung im Zustand T4 laserstrahlgeschweißt und anschließend warmausgelagert in den Zustand T6 sowie laserstrahlgeschweißt im Zustand T6 und definiert kaltausgelagert.

Figure 7. An example of fatigue crack appearance for “crack parallel to the weld” on the side of AA6056, laser beam welded in the T6 condition. Note that whereas the crack at the interface is nearly straight, deviation and deflection is observed at other locations in AA6056.

Abbildung 7. Beispiele für den Verlauf des Ermüdungsrisses parallel zur Schweißnaht auf der AA6056-Seite, laserstrahlgeschweißt im Zustand T6. Der Riss an der Grenzfläche ist nahezu geradlinig, dagegen weist der Riss in anderen Bereichen Abweichungen in den Aluminiumwerkstoff auf.

Figure 8. Typical differences in the fractographic mode during fatigue crack propagation in AA6056-T6 (a and b) and in the weld (c and d). Whereas the crack in the base material propagates in the striation mode, the tear mode is also observed in the weld ("crack parallel to the weld" in the fusion zone, laser beam welded in the T4 condition followed by post weld heat treatment T6).

Abbildung 8. Typische mikrofraktographische Unterschiede bei der Ermüdungsrissausbreitung im Grundwerkstoff AA6056-T6 (a, b) und der Laserstrahlschweißnaht (c, d) in AA6056. Im Vergleich zu Streifen im Grundwerkstoff weist die Schweißnaht zusätzlich auch Waben auf. (Orientierung "Riss parallel zur Schweißnaht", laserstrahlgeschweißt im Zustand T4 und anschließend warmausgelagert in den Zustand T6).

Figure 9. Fragments of AA6056 at the interface on the Ti6Al4V fracture half for "crack parallel to the weld", laser beam welded in the T4 condition followed by post weld heat treatment T6 (a), and in the T6 condition and defined naturally aged (b). Note also heavy deformation traces before macro-pores are cut by the fatigue crack front in (c), laser beam welded in the T6 condition and defined naturally aged.

Abbildung 9. Aluminium-Fragmente auf der Grenzfläche der Ti6Al4V-Seite mit der Orientierung "Riss parallel zur Schweißnaht", laserstrahlgeschweißt im Zustand T4 und anschließend warmausgelagert in den Zustand T6 (a) und laserstrahlgeschweißt im Zustand T6 und definiert kaltausgelagert (b). In (c) sind deutliche Verformungsspuren zu erkennen, bevor die Ermüdungsrissfront die Pore durchtrennt, laserstrahlgeschweißt im Zustand T6 und definiert kaltausgelagert.

Figure 10. Fatigue crack propagation for "crack perpendicular to the weld", from AA6056 towards Ti6Al4V, laser beam welded in the T4 condition followed by post weld heat treatment T6, and in the T6 condition and defined naturally aged. The tendency of unstable fracture along the interface when the crack hits the interface is indicated by horizontal arrows on the data points, and is shown in the inset. The locations of the

heat affected zone (7 mm), the fusion zone (3 mm) and the interface are indicated by horizontal gray coloured lines.

Abbildung 10. Ermüdungsrissausbreitung mit Orientierung “Riss senkrecht zur Schweißnaht” von der AA6056- zur Ti6Al4V-Seite, laserstrahlgeschweißt im Zustand T4 und anschließend warmausgelagert in den Zustand T6 und laserstrahlgeschweißt im Zustand T6 und definiert kaltausgelagert. Die Tendenz zum instabilen Bruch an der Grenzfläche ist durch horizontale Pfeile auf den Messpunkten gekennzeichnet. Instabiles Bruchverhalten trat ein, wenn der Riss auf die Grenzfläche traf, wie im eingefügten Bild zu erkennen ist. Die grauen Linien zeigen die Positionen bei der Wärmeeinflusszone (7 mm), der Schmelzzone (3 mm) und der Grenzfläche an.

Figure 11. Fatigue crack propagation for “crack perpendicular to the weld”, from Ti6Al4V towards AA6056. The tendency of crack non-propagation at various ΔK levels is indicated on the data points near the X-axis by the downward arrows.

Abbildung 11. Ermüdungsrissausbreitung mit Orientierung “Riss senkrecht zur Schweißnaht” von der Ti6Al4V- zur AA6056-Seite. Die nahe der X-Achse liegenden Messpunkte und die nach unten zeigenden Pfeile deuten die Tendenz des Rissstillstands bei verschiedenen ΔK-Werten an.

Figure 12. Resistance to fracture in terms of CTOD at various locations of the dissimilar joint laser beam welded in T4 followed by post weld heat treatment T6 (open symbols) and laser beam welded in T6 and defined naturally aged (filled symbols). CTOD values for the base materials are shown as bands for comparison. The three locations from the interface on the AA6056 side are shown schematically in the inset at the top-left. Location of the CTOD δ_5 gauge is shown in the inset at the bottom-right (after D. Hellmann/GKSS).

Abbildung 12. Bruchzähigkeit anhand von CTOD ermittelt an Proben mit unterschiedlichen Risspositionen. Die offenen Symbole repräsentieren die im Zustand T4 laserstrahlgeschweißte und anschließend in den Zustand T6 warmausgelagerte Verbindung, die geschlossenen Symbole repräsentieren die im Zustand T6 laserstrahlgeschweißte und definiert kaltausgelagerte Verbindung. Zum Vergleich sind die CTOD-Werte der Grundwerkstoffe als Bereich dargestellt. Das oben links eingefügte Bild zeigt die verschiedenen Risspositionen auf der AA6056-Seite. Die Lage

des Dehnungsmessaufnehmers zur Messung der Rissspitzenöffnung ist unten rechts dargestellt (nach D. Hellmann/GKSS).

Figure 13. Difference in the fracture mode at the interface and in the (primary) heat affected zone towards the base material (7 mm from the interface) for laser beam welded in T4 followed by post weld heat treatment T6 (a, b) and laser beam welded in T6 and defined naturally aged (c, d).

Abbildung 13. Unterschied im Bruchmodus an der Grenzfläche und in der (primären) Wärmeeinflusszone (7 mm Abstand von der Grenzfläche); a, b: laserstrahlgeschweißt im Zustand T4 und anschließend warmausgelagert in den Zustand T6; c, d: laserstrahlgeschweißt im Zustand T6 und definiert kaltausgelagert.

Figure 14. Resistance to fracture in terms of CTOD for “crack perpendicular to the weld”. CTOD values for the base materials are shown as bands for comparison.

Abbildung 14. Bruchzähigkeit anhand von CTOD ermittelt an Proben mit “Riss senkrecht zur Schweißnaht“. Die CTOD-Werte für die Grundwerkstoffe sind zum Vergleich als Bereich dargestellt.

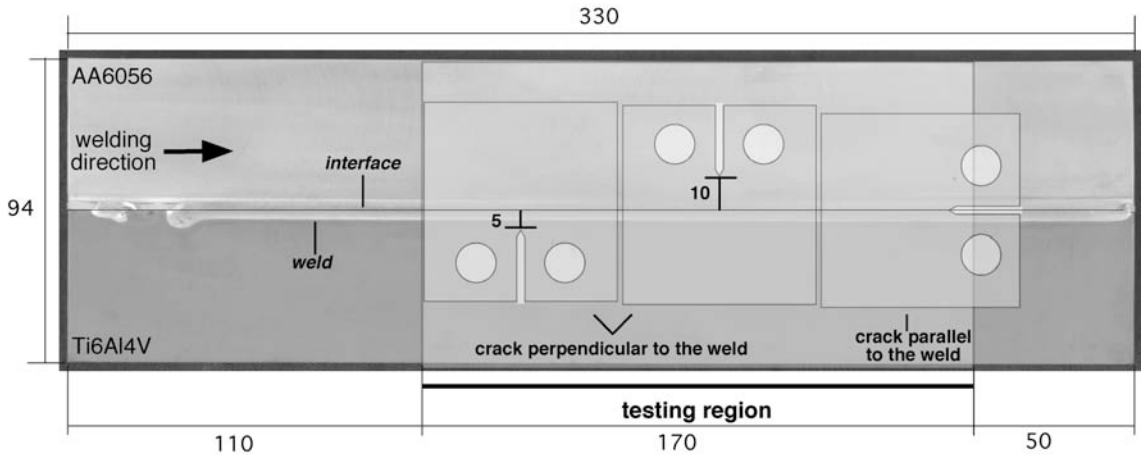

Figure 1. Location of fatigue crack propagation specimens with “crack parallel to the weld” and “crack perpendicular to the weld”. Specimens for fracture toughness were extracted similarly. (Dimensions in mm).

Abbildung 1. Probenentnahme für Ermüdungsrissausbreitungsversuche mit den Orientierungen “Riss parallel zur Schweißnaht” und “Riss senkrecht zur Schweißnaht”. Die Proben zur Bestimmung der Bruchzähigkeit wurden auf ähnliche Weise entnommen (Maße in mm).

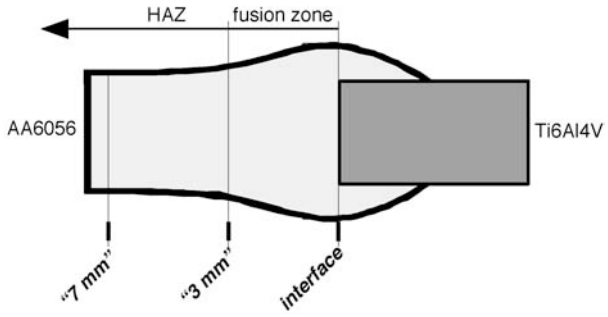

Figure 2. Relative location of sites for “crack parallel to the weld”, at which notable changes in microstructure, hardness, strength and deformation behaviour were observed. Vertical lines denote the sites which were notched for fatigue crack propagation and fracture testing. The continuation of the primary heat affected zone as a secondary zone is indicated by the arrow.

Abbildung 2. Die verschiedenen Bereiche auf der Al-Seite, in denen hinsichtlich Festigkeit, Härte und Gefüge Änderungen beobachtet wurden, sind durch vertikale Linien gekennzeichnet. Diese entsprechen Positionen auf den Proben für Ermüdungsrissausbreitungs- und Bruchmechanikversuche, in welche Kerben und Risse künstlich eingebracht wurden.

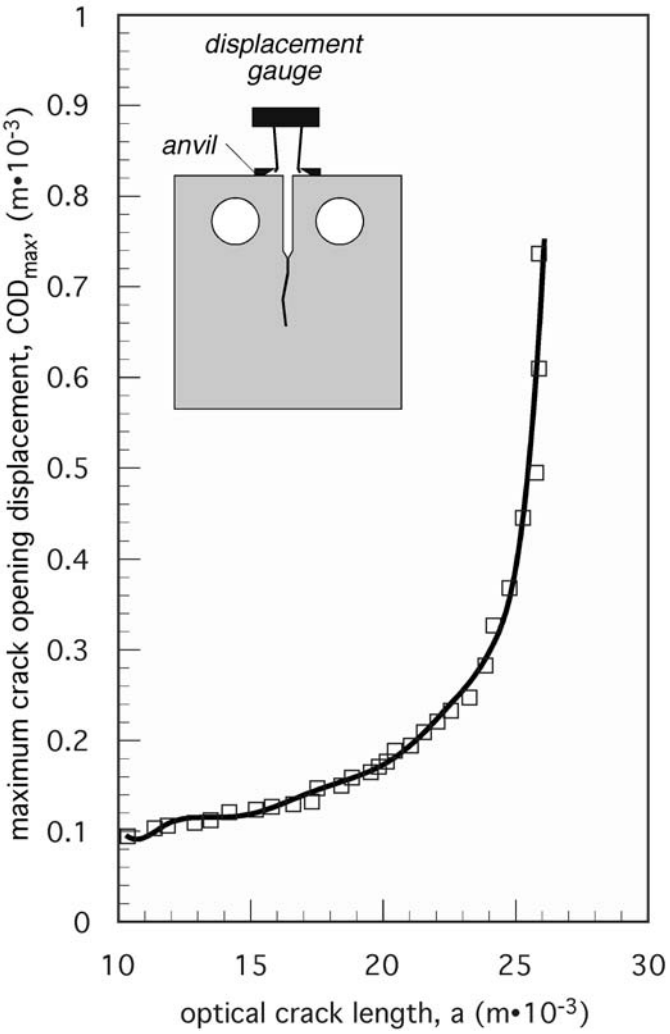

Figure 3. A typical example of the relationship between the maximum crack opening displacement and the optical crack length during fatigue crack propagation in a laser beam welded specimen in T6 with “crack parallel to the weld” and in the fusion zone. The fitted polynomial was used as the calibration curve for indirect crack length measurement. The position of the displacement gauge is shown in the inset.

Abbildung 3. Ein typisches Beispiel für die Beziehung zwischen maximaler Rissöffnung und Rissverlängerung während der Ermüdungsrissausbreitung in einer im Zustand T6 laserstrahlgeschweißten Probe mit der Orientierung “Riss parallel zur Schweißnaht”. Für eine indirekte Risslängenmessung wurde die durch ein Polynom angepasste Kurve zur Kalibration herangezogen. Das eingefügte Bild zeigt schematisch die Lage des Dehnungsmessaufnehmers.

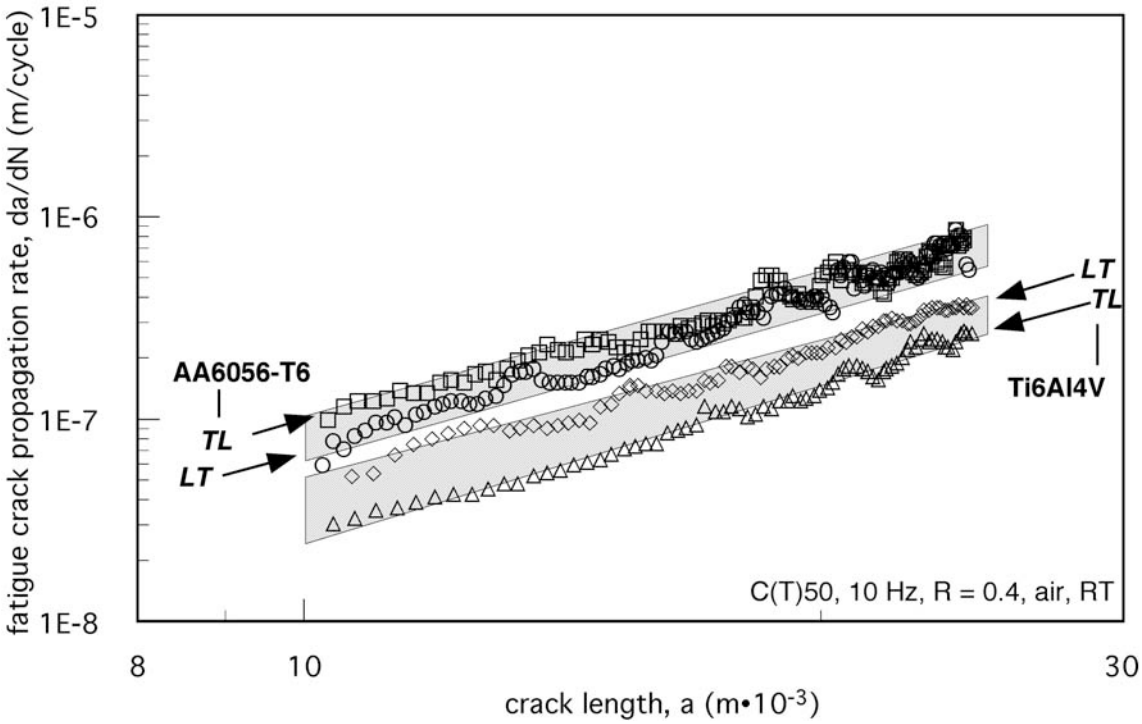

Figure 4. Fatigue crack propagation behaviour of the base materials along the rolling direction (TL orientation) and perpendicular to it (LT orientation). The range of fatigue crack propagation of the base materials is shown by hatching and is used for comparison in the diagrams to follow.

Abbildung 4. Ermüdungsrissausbreitung in den Grundwerkstoffen parallel zur Walzrichtung (TL) und quer zur Walzrichtung (LT). Der jeweilige Bereich der Ermüdungsrissausbreitung ist schattiert hervorgehoben und wird in nachfolgenden Diagrammen zur besseren Vergleichbarkeit hinterlegt.

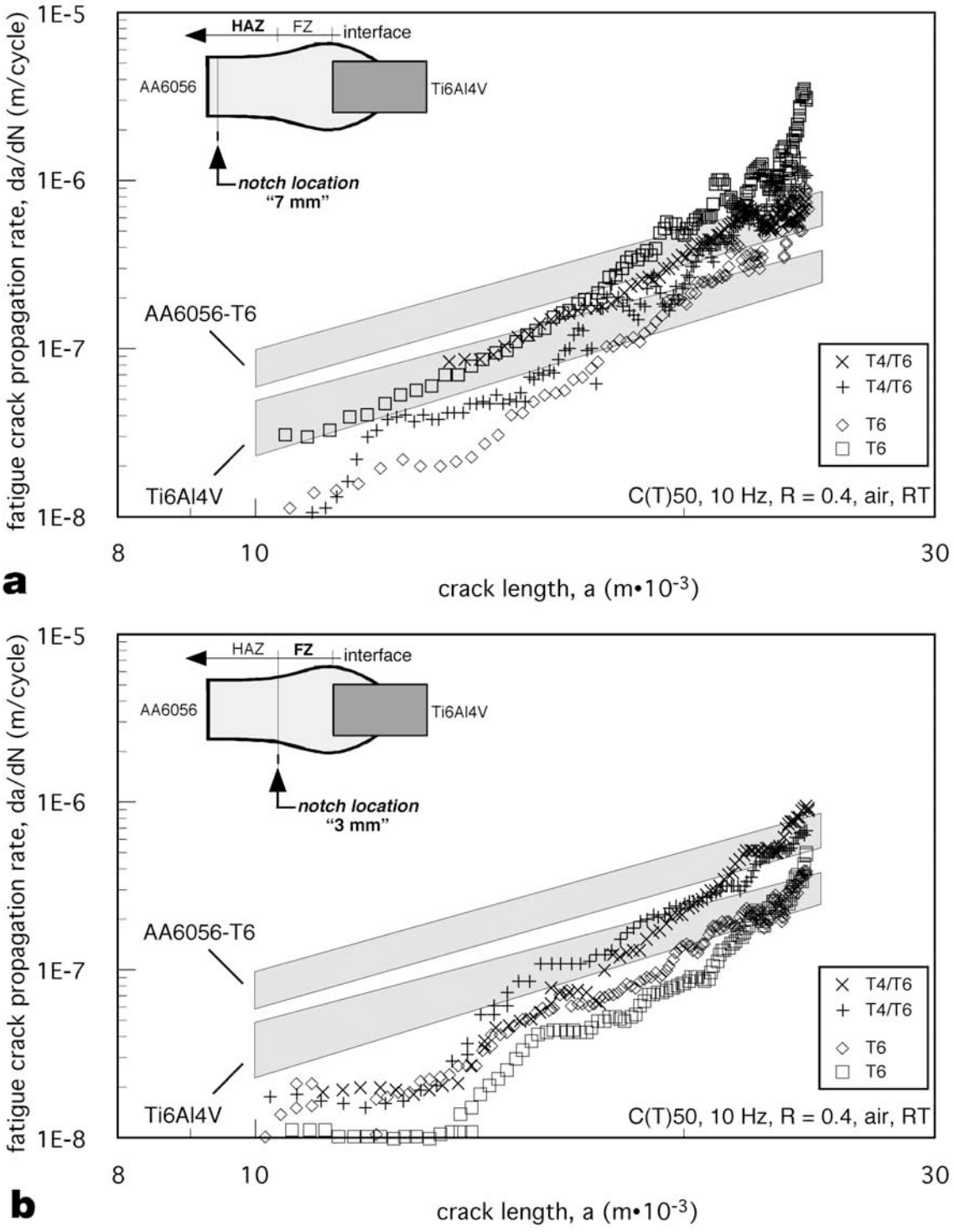

Figure 5. Fatigue crack propagation behaviour for "crack parallel to the weld" at the locations shown in the insets on the side of AA6056, laser beam welded in the T4 condition followed by post weld heat treatment T6, and welded in the T6 condition and defined naturally aged for notch location "7 mm from the interface" (a), and "3 mm from the interface" (b).

Abbildung 5. Ermüdungsrissausbreitung parallel zur Schweißnaht in verschiedenen Risspositionen bei 7 mm (a) und 3 mm (b) auf der AA6056-Seite, im Zustand T4 laserstrahlgeschweißt und anschließend warmausgelagert in den Zustand T6 sowie laserstrahlgeschweißt im Zustand T6 und definiert kaltausgelagert.

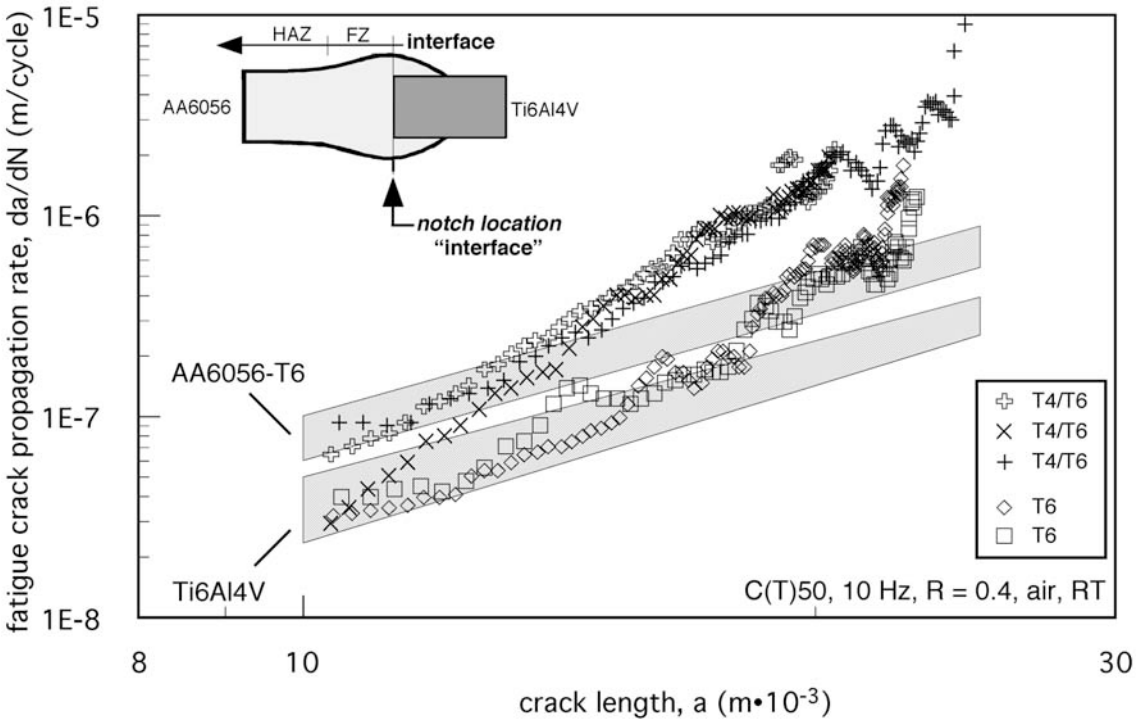

Figure 6. Fatigue crack propagation behaviour for “crack parallel to the weld” at the interface, laser beam welded in the T4 condition followed by post weld heat treatment T6, and welded in the T6 condition and defined naturally aged.

Abbildung 6. Ermüdungsrissausbreitung parallel zur Schweißnaht an der Grenzfläche der Verbindung im Zustand T4 laserstrahlgeschweißt und anschließend warmausgelagert in den Zustand T6 sowie laserstrahlgeschweißt im Zustand T6 und definiert kaltausgelagert.

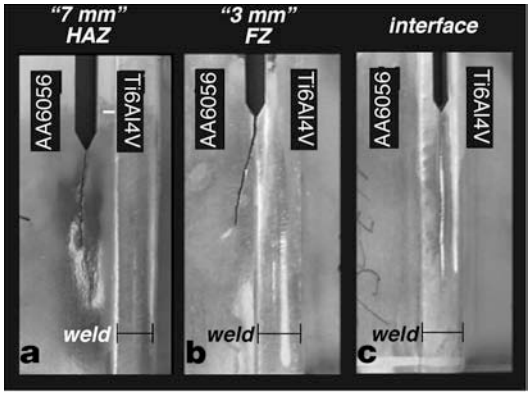

Figure 7. An example of fatigue crack appearance for "crack parallel to the weld" on the side of AA6056, laser beam welded in the T6 condition. Note that whereas the crack at the interface is nearly straight, deviation and deflection is observed at other locations in AA6056.

Abbildung 7. Beispiele für den Verlauf des Ermüdungsrisses parallel zur Schweißnaht auf der AA6056-Seite, laserstrahlgeschweißt im Zustand T6. Der Riss an der Grenzfläche ist nahezu geradlinig, dagegen weist der Riss in anderen Bereichen Abweichungen in den Aluminiumwerkstoff auf.

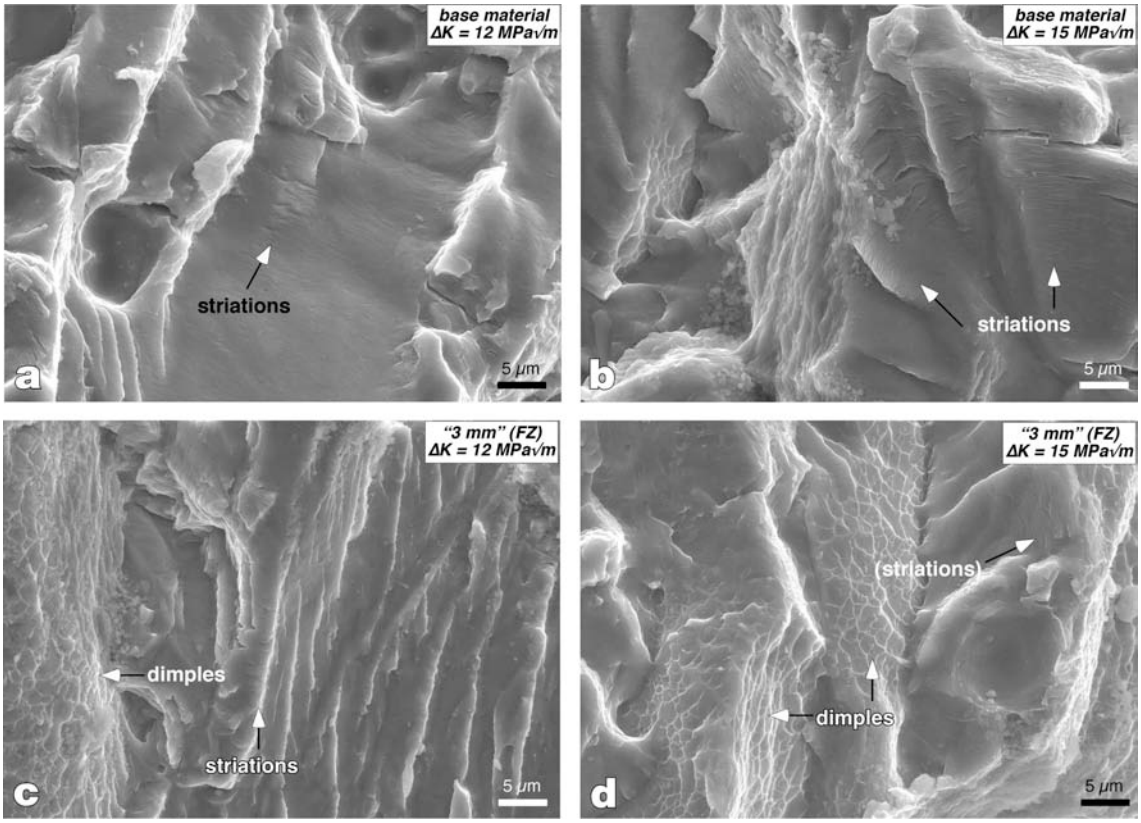

Figure 8. Typical differences in the fractographic mode during fatigue crack propagation in AA6056-T6 (a and b) and in the weld (c and d). Whereas the crack in the base material propagates in the striation mode, the tear mode is also observed in the weld ("crack parallel to the weld" in the fusion zone, laser beam welded in the T4 condition followed by post weld heat treatment T6).

Abbildung 8. Typische mikrofraktographische Unterschiede bei der Ermüdungsrissausbreitung im Grundwerkstoff AA6056-T6 (a, b) und der Laserstrahlschweißnaht (c, d) in AA6056. Im Vergleich zu Streifen im Grundwerkstoff weist die Schweißnaht zusätzlich auch Waben auf. (Orientierung "Riss parallel zur Schweißnaht", laserstrahlgeschweißt im Zustand T4 und anschließend warmausgelagert in den Zustand T6).

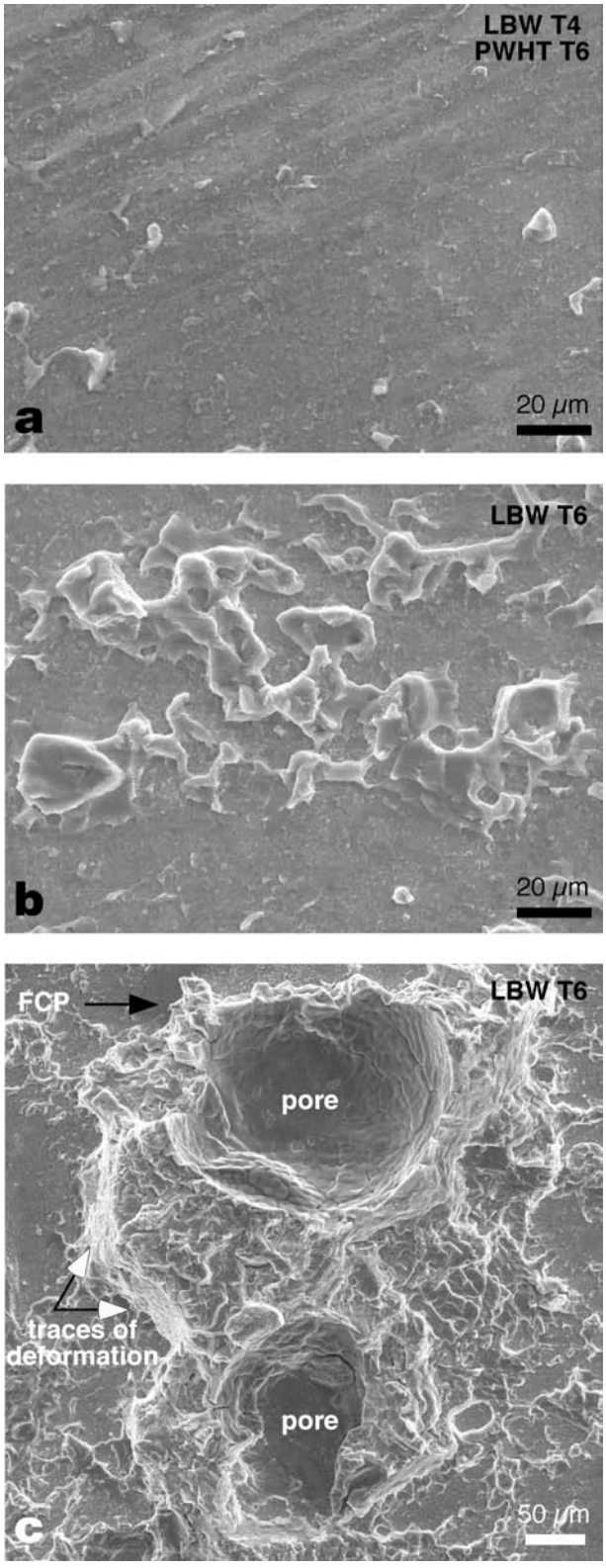

Figure 9. Fragments of AA6056 at the interface on the Ti6Al4V fracture half for “crack parallel to the weld”, laser beam welded in the T4 condition followed by post weld heat treatment T6 (a), and in the T6 condition and defined naturally aged (b). Note also

heavy deformation traces before macro-pores are cut by the fatigue crack front in (c), laser beam welded in the T6 condition and defined naturally aged.

Abbildung 9. Aluminium-Fragmente auf der Grenzfläche der Ti6Al4V-Seite mit der Orientierung “Riss parallel zur Schweißnaht“, laserstrahlgeschweißt im Zustand T4 und anschließend warmausgelagert in den Zustand T6 (a) und laserstrahlgeschweißt im Zustand T6 und definiert kaltausgelagert (b). In (c) sind deutliche Verformungsspuren zu erkennen, bevor die Ermüdungsrissfront die Pore durchtrennt, laserstrahlgeschweißt im Zustand T6 und definiert kaltausgelagert.

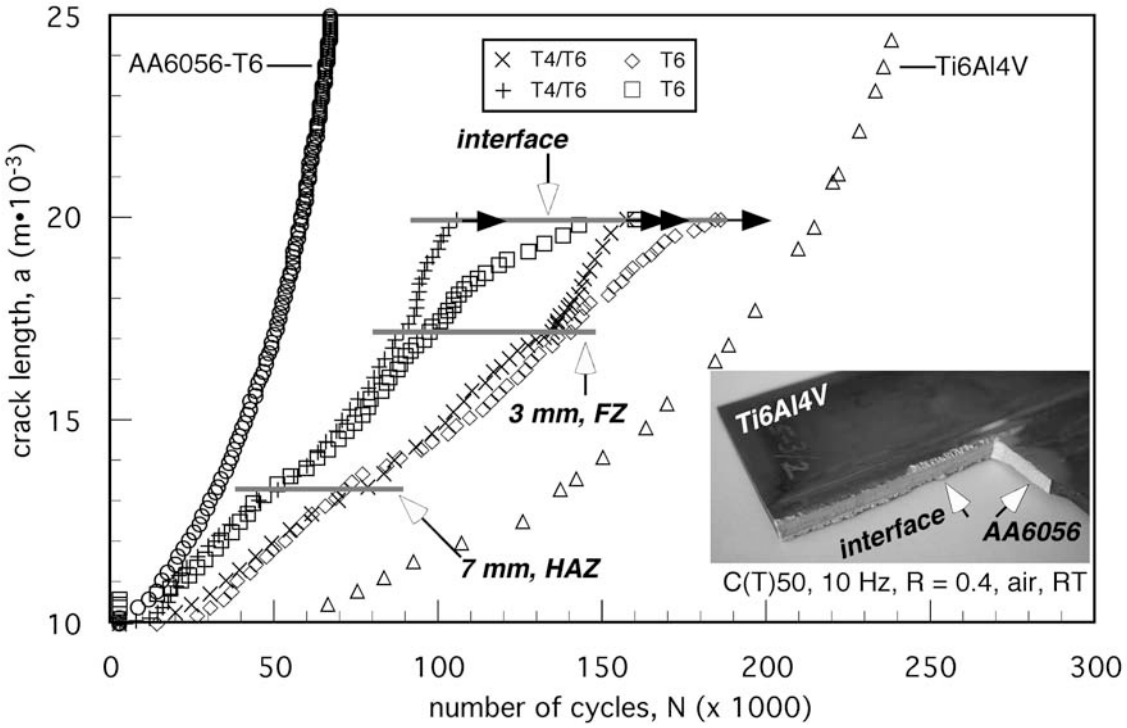

Figure 10. Fatigue crack propagation for “crack perpendicular to the weld”, from AA6056 towards Ti6Al4V, laser beam welded in the T4 condition followed by post weld heat treatment T6, and in the T6 condition and defined naturally aged. The tendency of unstable fracture along the interface when the crack hits the interface is indicated by horizontal arrows on the data points, and is shown in the inset. The locations of the heat affected zone (7 mm), the fusion zone (3 mm) and the interface are indicated by horizontal gray coloured lines.

Abbildung 10. Ermüdungsrissausbreitung mit Orientierung “Riss senkrecht zur Schweißnaht” von der AA6056- zur Ti6Al4V-Seite, laserstrahlgeschweißt im Zustand T4 und anschließend warmausgelagert in den Zustand T6 und laserstrahlgeschweißt im Zustand T6 und definiert kaltausgelagert. Die Tendenz zum instabilen Bruch an der Grenzfläche ist durch horizontale Pfeile auf den Messpunkten gekennzeichnet. Instabiles Bruchverhalten trat ein, wenn der Riss auf die Grenzfläche traf, wie im eingefügten Bild zu erkennen ist. Die grauen Linien zeigen die Positionen bei der Wärmeeinflusszone (7 mm), der Schmelzzone (3 mm) und der Grenzfläche an.

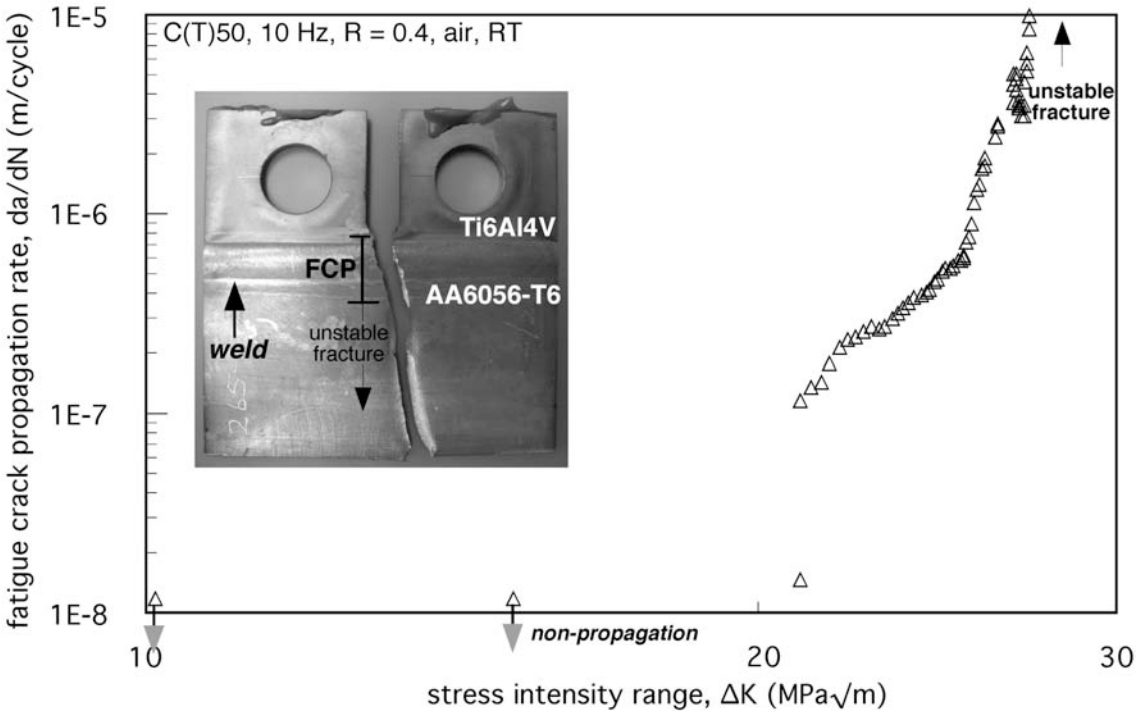

Figure 11. Fatigue crack propagation for “crack perpendicular to the weld”, from Ti6Al4V towards AA6056. The tendency of crack non-propagation at various ΔK levels is indicated on the data points near the X-axis by the downward arrows.

Abbildung 11. Ermüdungsrissausbreitung mit Orientierung “Riss senkrecht zur Schweißnaht” von der Ti6Al4V- zur AA6056-Seite. Die nahe der X-Achse liegenden Messpunkte und die nach unten zeigenden Pfeile deuten die Tendenz des Rissstillstands bei verschiedenen ΔK-Werten an.

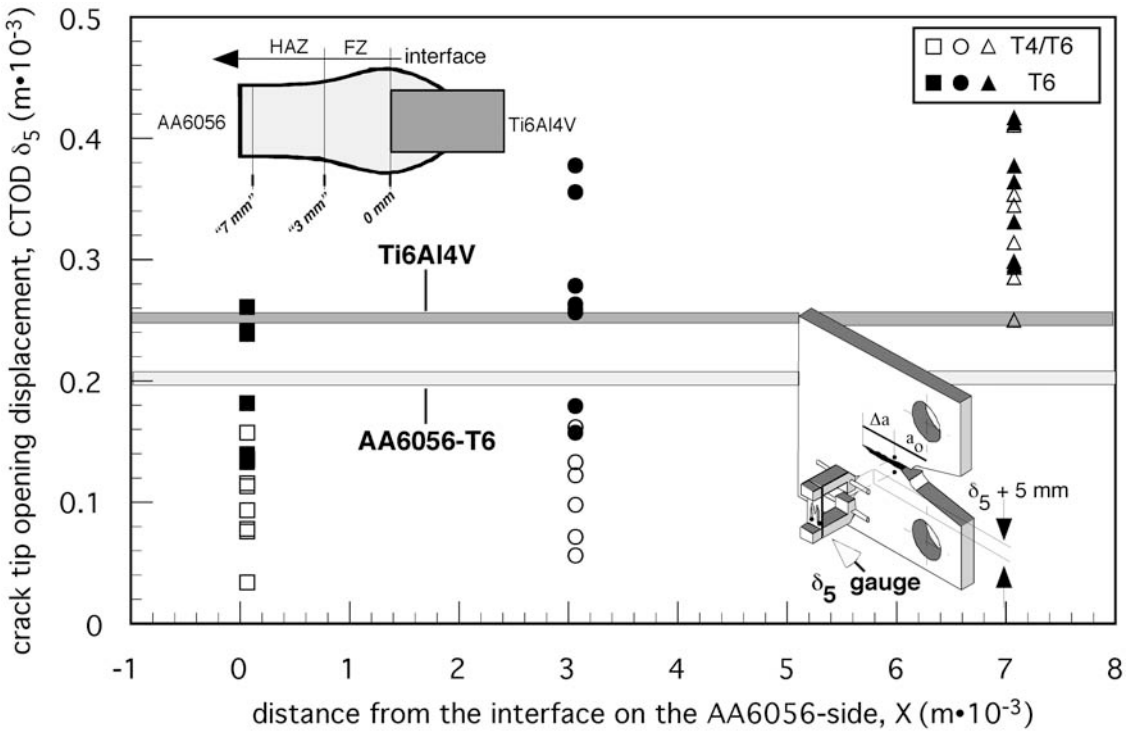

Figure 12. Resistance to fracture in terms of CTOD at various locations of the dissimilar joint laser beam welded in T4 followed by post weld heat treatment T6 (open symbols) and laser beam welded in T6 and defined naturally aged (filled symbols). CTOD values for the base materials are shown as bands for comparison. The three locations from the interface on the AA6056 side are shown schematically in the inset at the top-left. Location of the CTOD δ_5 gauge is shown in the inset at the bottom-right (after D. Hellmann/GKSS).

Abbildung 12. Bruchzähigkeit anhand von CTOD ermittelt an Proben mit unterschiedlichen Risspositionen. Die offenen Symbole repräsentieren die im Zustand T4 laserstrahlgeschweißte und anschließend in den Zustand T6 warmausgelagerte Verbindung, die geschlossenen Symbole repräsentieren die im Zustand T6 laserstrahlgeschweißte und definiert kaltausgelagerte Verbindung. Zum Vergleich sind die CTOD-Werte der Grundwerkstoffe als Bereich dargestellt. Das oben links eingefügte Bild zeigt die verschiedenen Risspositionen auf der AA6056-Seite. Die Lage des Dehnungsmessaufnehmers zur Messung der Rissspitzenöffnung ist unten rechts dargestellt (nach D. Hellmann/GKSS).

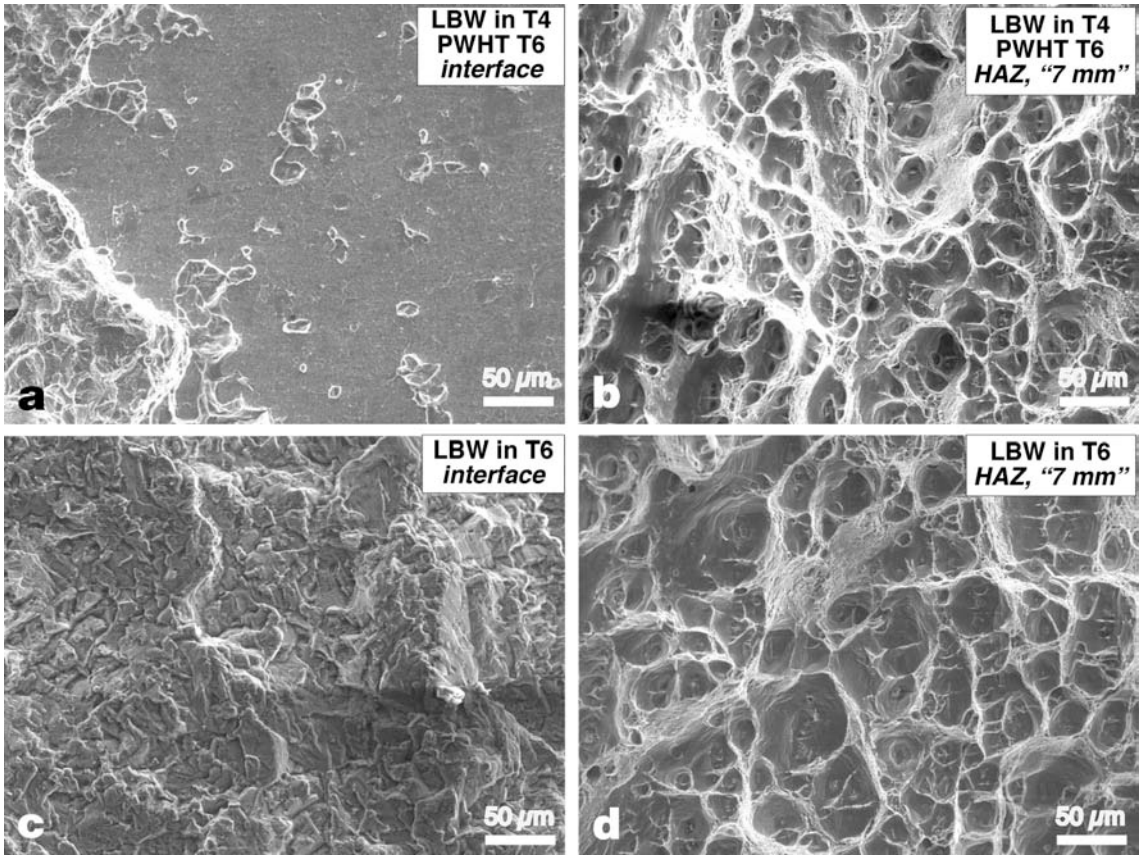

Figure 13. Difference in the fracture mode at the interface and in the (primary) heat affected zone towards the base material (7 mm from the interface) for laser beam welded in T4 followed by post weld heat treatment T6 (a, b) and laser beam welded in T6 and defined naturally aged (c, d).

Abbildung 13. Unterschied im Bruchmodus an der Grenzfläche und in der (primären) Wärmeeinflusszone (7 mm Abstand von der Grenzfläche); a, b: laserstrahlgeschweißt im Zustand T4 und anschließend warmausgelagert in den Zustand T6; c, d: laserstrahlgeschweißt im Zustand T6 und definiert kaltausgelagert.

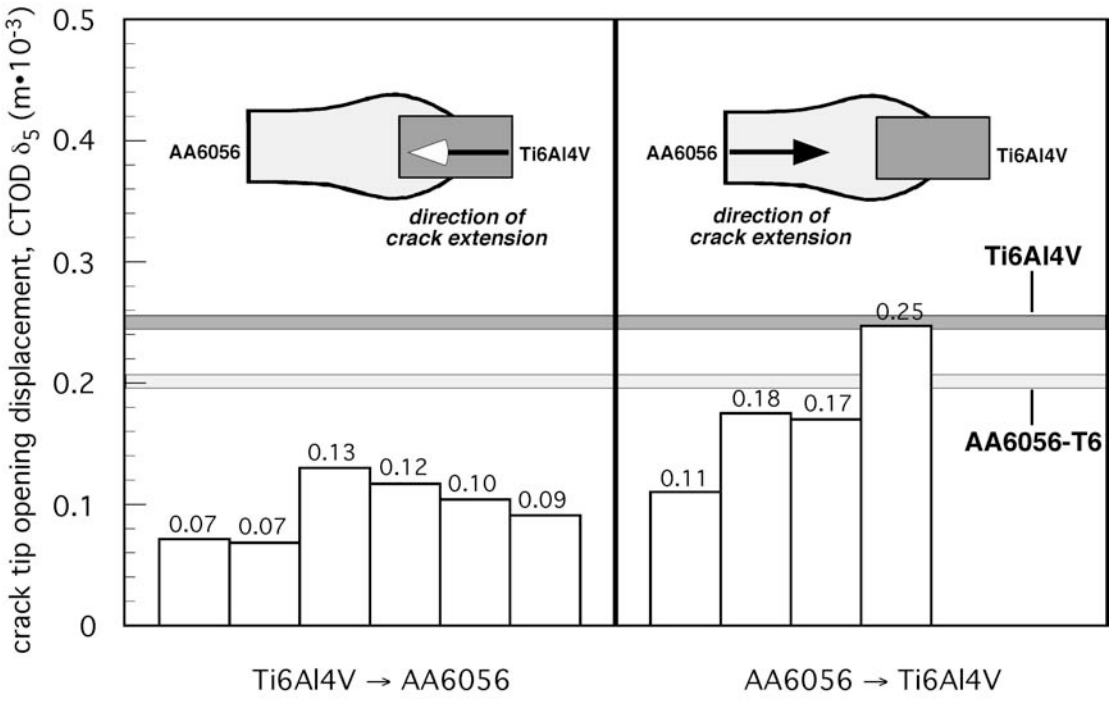

Figure 14. Resistance to fracture in terms of CTOD for “crack perpendicular to the weld”. CTOD values for the base materials are shown as bands for comparison.

Abbildung 14. Bruchzähigkeit anhand von CTOD ermittelt an Proben mit “Riss senkrecht zur Schweißnaht“. Die CTOD-Werte für die Grundwerkstoffe sind zum Vergleich als Bereich dargestellt.